2018

Thermo-Hydraulic Model for Steam Condensation in a Large, Inclined, Flattened-Tube Air-Cooled Condenser

William A. Davies
ACRC, University of Illinois, United States of America, daviesi2@illinois.edu

Predrag S. Hrnjak
pega@illinois.edu

Thermo-hydraulic model for steam condensation in a large, inclined, flattened-tube air-cooled condenser

William A. DAVIES III[1], Pega HRNJAK[1,2]*

[1]University of Illinois at Urbana-Champaign,
Department of Science and Engineering,
Urbana, IL, USA
daviesi2@illinois.edu, pega@illinois.edu

[2]Creative Thermal Solutions,
Urbana, IL, USA

* Corresponding Author

ABSTRACT

A thermo-hydraulic model for calculating capacity, heat transfer coefficient and void fraction of an inclined air-cooled steam condenser is presented. The condenser tube has an elongated-slot cross-section, with inner dimensions of 214 x 16 mm. The tube is 10.7 m long. The model is for downward inclination angles from 0-90°, with co-current vapor and condensate flow. The cooling air is in cross flow.

This model is developed based on existing models for inclined, stratified-flow condensation. These have been adapted to the flattened-tube air-cooled condenser geometry and conditions. The model couples both air- and steam-side behavior in order to accurately resolve the variation in heat transfer coefficients, temperature difference, and heat flux. On the steam side, the model is for stratified flow, and separates the flow into two sections: a falling film along the wall, and an axially-flowing condensate river along the tube bottom. The axially-flowing condensate river is modeled using open-channel-flow theory. On the air side, heat transfer coefficient is determined from a combination of empirical correlation and CFD.

The model and experimental results show agreement within 5% in capacity and overall heat transfer coefficient for all tube inclinations.

1. INTRODUCTION

Condenser thermal performance is commonly predicted using one-dimensional models (e.g. (Li & Hrnjak, 2017)). Cold- and hot-side heat transfer coefficients (HTCs) are predicted along the length of the condenser using correlations and assumptions of constant heat flux or wall temperature. Corrections are then made for development lengths (Mills, 1962), or for changes in temperature difference (Yamashita, Izumi, & Yamaguchi, 1977). This method is effective for cases where one or both HTCs are constant. However, Sparrow *et al.* (2013) have found that when the HTC of both fluids is not constant, the assumptions of constant temperature difference or constant heat flux break down, and significant inaccuracy in prediction of overall HTC can result.

For an air-cooled condenser (ACC), the HTCs on the steam and air sides vary significantly both in the axial and cross-flow directions. For the steam side in particular, The HTC can vary by over two orders of magnitude in a tube cross-section, from the liquid condensate at the tube bottom to the high-quality vapor at the tube top. For this type of condenser – with a large, flattened-tube geometry – heat flux and temperature difference also vary in the axial and cross-flow directions. Therefore, a local model for heat transfer is required. Several such models have been proposed in literature for condensation. Chato (1960) divided the stratified flow regime into two regions for heat transfer – the falling film on the tube wall, and the axially-flowing condensate at the tube bottom. He used an open-channel-flow model to predict depth of the condensate, but considered heat transfer through this layer to be negligible. For the falling film, he used a model based on Nusselt (1916) analysis to predict HTC. Dobson and Chato (1998) further

refined this model to account for convective heat transfer in the stratified condensate layer. Saffari and Naziri (2010) used a numerical model to predict HTC in stratified flow. Like Chato, they divided the flow into two regions, and found good agreement with the correlation of Wang and Ma (1991). Lips and Meyer (2012) also used a separated model for stratified condensation in a circular tube. Unlike the model of Chato, they determined void fraction with a pressure-driven-flow model based on that of Taitel and Dukler (1976). In addition, they approximated the heat transfer through the river as one-dimensional conduction, neglecting the convective contribution.

Other researchers have used a continuous-film model instead of dividing the flow into two regions. Hussein *et al.* (2001) developed this type of model for an inclined thermosiphon. Kekaula *et al.* (2017) used a continuous numerical model to determine the steam-side performance of round-tube ACCs. Notably, they also coupled air-side and steam-side behavior. On the air side, CFD simulations were used to determine the cross-flow Nusselt number over a tube bundle. In this paper, the thermo-hydraulic model separates the flow into two regions. In addition, the model couples air- and steam-side behavior.

When considering separated models, the determination of condensate depth requires further comment. Significant research has been performed on this topic, and several models have been developed for round tubes. Traditional void fraction correlations for condensation, such as that of Taitel and Dukler (1976), assume pressure-driven flow, where pressure drop through each phase and slip ratio between the phases are the important parameters. However, these models can have errors for low-mass-flux gravity-driven flows, where the pressure drops through the vapor and liquid are negligible and do not affect the void fraction.

In the ACC, with gravity-driven flow, the situation is similar to a lateral spillway, where void fraction depends greatly on tube inclination and heat flux. Spatially-varied open-channel-flow models can be used for these flows. Chow (1959) described an early solution to this problem when developing his open-channel-flow framework. Kao (1974) specifically analyzed the problem of spatially-varied flow, both experimentally and numerically. Kao's model accurately predicted the water surface profile when varying several parameters, including channel slope, discharge, and lateral inflow rate. Lateral inflow rate was found to have the largest effect on the water surface profile. Yen (1971) derived the spatially-varied flow equations from first principles. He then analyzed the common assumptions used in these models under different flow conditions. He found the conventionally-used equations to be simplifications of special cases of the general spatially-varied flow equations.

This study models the void fraction using a spatially-varied open-channel-flow model and compares the model to experimental results.

2. CONDENSER TUBE AND FACILITY

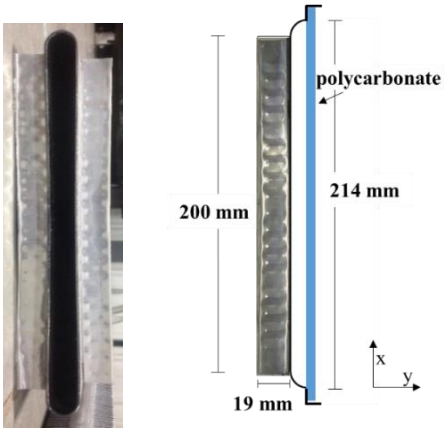

Figure 1: Cross-section views of full tube and tube that has been cut along the centerline. A polycarbonate window allows visualization along the tube length.

The model is based on the condenser tube that is described in detail in Davies *et al.* (2018). The tube is 10.7 m in length, 0.214 m in inner height, and 0.016 m in inner width. The tube wall is steel with aluminum cladding on the outside, and the wavy fins are aluminum. The fins are 200 mm x 19 mm. For the experiment, the condenser tube is cut in half along the vertical center-line and a polycarbonate window is installed to allow visual access. The polycarbonate window is held adiabatic. The model is used to predict river depth and condenser capacity for this half tube, in order to compare with the experiment results. Figure 1 shows the geometry of the tube both before and after the cut.

A complete description of the experimental procedure and void fraction results is also presented in Kang *et al.* (2017) so the details are not presented here. Experiment results for capacity, overall HTC, and condensate river depth are presented here for comparison to the model.

3. MODEL OF THE CONDENSATE RIVER

The axially-flowing condensate river is modeled as a spatially-varied open channel flow. Due to the large cross-sectional area of the tube, the surface of the condensate river is unconstrained, and free to arrange itself based on the balance of gravitational, pressure, shear, and surface tension forces.

To begin the model, the flow must be characterized as sub- or super-critical. A subcritical flow is characterized by lower velocity and greater depth of the condensate river, and occurs at lower inclinations. The depth of subcritical flows is controlled by the downstream (outlet) conditions. Supercritical flows have greater velocity, and their depth is controlled by the upstream (inlet) conditions. The Froude number (equation (1)) is the criterion for determining criticality, with subcritical flows having Fr < 1 and supercritical flows having Fr > 1.

For this type of flow, the inlet and outlet conditions are important. Here, the inlet condition is a falling condensate film, so the initial depth of the condensate river is the film thickness at tube bottom. At the outlet, the condensate exits the tube via a free overfall. For the model, the river depth is initially assumed to be equal to the critical depth (Fr = 1) at the tube outlet. The river depth is then calculated for a short distance upstream. If the depth increases in the upstream direction, the flow is subcritical, and the calculation can continue in the upstream direction. If the depth decreases, then the flow is supercritical, and the calculation must begin from the tube inlet.

In order to determine the critical depth at the tube outlet, the Froude number is set equal to one:

$$Fr_{critical} = \frac{v_{c,critical}}{\sqrt{gD_{h,critical}}} = 1 \tag{1}$$

$$D_{h,critical} = \left(\frac{\dot{V}^2}{gW_{top,critical}^2} \right)^{1/3} \tag{2}$$

$$D_h = \frac{A_{cs}}{W_t} \tag{3}$$

$$v_c = \frac{\dot{V}_c}{A_{cs}} \tag{4}$$

The top width of the river is defined as the width of the free surface. For a semi-circular channel, this width is a function of the depth of the condensate. Therefore, the top width is initially assumed to be the maximum channel width, and equation (2) is solved iteratively.

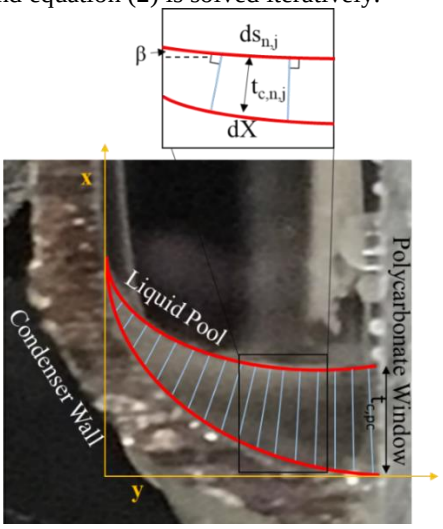

Figure 2: Condensate layer discretized for model of thermal conduction

The cross-sectional profile of the condensate surface is determined by a model similar to that used by Lips and Meyer (2012), with the geometry adapted to match the condenser tube in this study. For each river depth, the cross-sectional area, the top width, and the wetted perimeter of the river are calculated. For this river surface model, the receding contact angle of water on the rusted steel wall is assumed to be 0°. This was measured with a goniometer in independent testing.

For the model, shear forces are considered to be negligible, and the shape of the interface is controlled by gravitational and surface-tension forces. The model proceeds by equating pressures. From the Young-Laplace equation describing the magnitude of the surface-tension force:

$$P_f(X) = P_g - \frac{\sigma}{r(X)} \tag{5}$$

Considering the effect of tube inclination ($\varphi = 0°$ for these experiments), the gravitational force is:

$$P_f(X) = -\left(\rho_f - \rho_g\right) g(\cos\varphi) X + P_f\left(X = t_{c,PC}\right) \tag{6}$$

Equating (5) and (6) and denoting the radius of curvature at the polycarbonate window as r_{pc}, yields:

$$\frac{\sigma}{r_{PC}} - \frac{\sigma}{r(X)} = -\left(\rho_f - \rho_g\right) g\left(\cos\varphi\right) X \tag{7}$$

Equation (7) can be simplified to:

$$r(X) = \frac{1}{\frac{2X}{b^2} + \frac{1}{r_{PC}}} \tag{8}$$

Where b^2 is the capillary constant of the fluid:

$$b^2 = \frac{2\sigma}{\left(\rho_f - \rho_g\right) g \cos\varphi} \tag{9}$$

Geometry shows us that:

$$r(X) = \frac{dX}{\left(\sin\beta\right) d\beta} \tag{10}$$

Equating (8) and (10) yields:

$$\left(\frac{2X}{b^2} + \frac{1}{r_{PC}}\right) dX = \left(\sin\beta\right) d\beta \tag{11}$$

Integrating equation (11) from the polycarbonate window ($\beta = 0 \ @ \ X = t_{c,PC}$):

$$\left(\frac{X}{b}\right)^2 + \frac{X}{r_{PC}} = 1 - \cos\beta + \left(\frac{t_{c,PC}}{b}\right)^2 + \frac{t_{c,PC}}{r_{PC}} \tag{12}$$

The calculation is performed most easily by setting X = 0 m at the top of the condensate along the polycarbonate ($t_{c,pc}$). The surface profile can then be solved in an iterative scheme, beginning at the polycarbonate window. An initial radius of curvature, r_{pc}, is assumed, and the initial parameters are:

$$Y_1 = .00636\,\text{m};\ X_1 = 0\,\text{m};\ \beta_1 = 0^o$$

The subsequent coordinates are found as:

$$Y_{j+1} - Y_j = \left(\cos\beta_j\right) ds_j \tag{13}$$

$$X_{j+1} - X_j = \left(\sin\beta_j\right) ds_j \tag{14}$$

$$ds_j = r\left(X_j\right) d\beta_j \tag{15}$$

Subsequent values of β are then found using equation (12). The calculation proceeds until the condensate surface intersects the condenser wall. The boundary condition at the wall is a contact angle of 0°. An iterative process is used to satisfy this boundary condition, whereby r_{pc} is varied until the condensate surface and the wall are tangent at the point of intersection. The bottom of the condenser wall is a circular arc that subtends an angle of 90°.

Once the shape of the river surface is determined at the outlet, the calculation proceeds upstream. First, the volumetric flow rate of condensate is expected to vary linearly based on constant heat flux along the condenser length.

$$d\dot{V} = \frac{\dot{V}_{outlet}}{n} \tag{16}$$

Where *n* is the number of intervals along the condenser length. Looking at a small length of the condenser, *dz*, in Figure 3 the change in momentum along the river can be seen. Numerically, this is:

$$\Delta p = \rho\left(\dot{V} + d\dot{V}\right)\left(v + dv\right) - \rho\dot{V}v \tag{17}$$

This can be equated with the sum of the forces on the river:

$$\Delta p = \sum F = F_{gravity} + F_{wall} + F_{pressure} + F_{vapor} \tag{18}$$

Assuming that $dA_{cs}dz$ is small:

$$F_{gravity} \approx \rho g S_o A_{cs} dz \tag{19}$$

$$F_{wall} = -\rho g A_{cs} S_f dz \tag{20}$$

$$S_f = \frac{\dot{V}^2 n^2}{A_{cs}^2 R_h^{4/3}} \tag{21}$$

$$F_{pressure} = P_1 A_{cs} - P_2 A_{cs} = -\rho g A_{cs} dD_h \tag{22}$$

$$F_{vapor} = \tau_v W_{in} dz \tag{23}$$

$$\tau_v = \frac{f_{in}\rho_v\left(v_v - v_l\right)^2}{2} \tag{24}$$

Interfacial friction factor, f_i, is calculated using Taitel and Dukler's (Y Taitel & AE Dukler, 1976) formula:

$$f_{in} = \begin{cases} \dfrac{16}{\mathrm{Re}_v} \; if \; \mathrm{Re}_v < 2000 \\ .046\,\mathrm{Re}_v^{-0.2} \; if \; \mathrm{Re}_v \geq 2000 \end{cases} \tag{25}$$

Equating the change in momentum (17) with these forces, and neglecting the $d\dot{V}dv$ term on the left, yields:

$$\rho\left(\dot{V}dv + vd\dot{V}\right) = -\rho g A_{cs} dD_h + \tau_v W_{in} dz - \rho g A_{cs} S_f dz + \rho g S_o A_{cs} dz \tag{26}$$

Solving for the change in hydraulic depth yields:

$$dD_h = -\frac{1}{g}\left(vdv + \frac{v}{A_{cs}}d\dot{V}\right) + \left(\frac{\tau_v W_{in}}{\rho g A_{cs}} - S_f + S_o\right)dz \tag{27}$$

Further algebraic manipulation yields:

$$dD_h = -\frac{v}{g}\left(\frac{2A_{cs}d\dot{V} - \dot{V}dA_{cs} + dA_{cs}d\dot{V}}{A_{cs}^{\;2} + A_{cs}dA_{cs}}\right) + \left(\frac{\tau_v W_{in}}{\rho g A_{cs}} - S_f + S_o\right)dz \tag{28}$$

Then, it is assumed that small incremental changes in A_{cs} allows one to neglect $dA_{cs}d\dot{V}$ in the numerator and $A_{cs}dA_{cs}$ in the denominator. With some more algebra, and discretizing dD_h as ΔD_h, this yields a final equation of:

$$\Delta D_h = -\frac{\dot{V}_1\left(v_1 + v_2\right)}{g\left(\dot{V}_1 + \dot{V}_2\right)}\left(\Delta v + \frac{v_2\Delta\dot{V}}{\dot{V}_1}\right) + \left(\frac{\tau_v W_{in}}{\rho g A_{cs}} - S_f + S_o\right)\Delta z \tag{29}$$

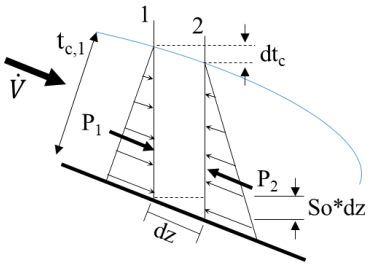

Figure 3: Differential step along the condenser length, showing change in forces and river height

For supercritical flow, the depth is controlled from upstream, so an inlet flow condition is needed. An assumption of zero depth at the inlet is valid physically, but leads to mathematical difficulty in beginning the iteration. For a close approximation, an alternative starting point is to use Nusselt analysis to calculate film thickness of the falling condensate film at the bottom of the condenser wall. For the annular flow at the condenser inlet, the thickness of the wall condensate is a valid starting approximation.

4. THERMAL MODEL

For the thermal model, the steam side is divided into two sections: the stratified condensate river flowing axially, and the thin film falling down the condenser wall. In the condensate river, the heat transfer mechanism is approximated as one-dimensional conduction. In the falling film, HTC is predicted by the theory of Nusselt (1916).

Inputs to the model are the air inlet temperature (T_{ai}), air velocity (v_a), steam temperature (T_s), and river depth along the condenser, which is calculated from the river model described above. First, condenser capacity is estimated for the given input conditions, and the river model is run. Then, the thermal model is run, taking this initial river depth as input. The capacity determined from the thermal model is compared to the initial capacity estimate. If the two values differ, the river model is re-run, and the thermal model is then re-run with the accurate river depths. This iterative process is continued until the modeled capacity does not change.

For the model, the condenser is divided along the length into 11 cross sections, *n*. Each section is 1 m long, except for the last section, which is 0.7 m long. Outputs calculated for each 1 m section are T_w, T_a, h_s , h_a, U, and Q.

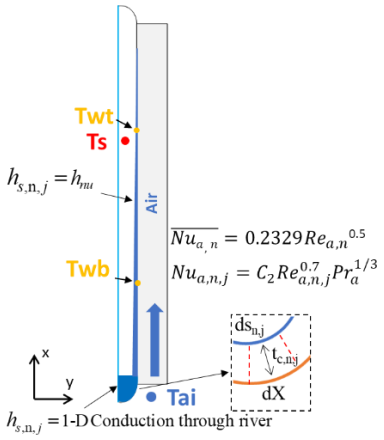

Figure 4: Scheme of the thermal model

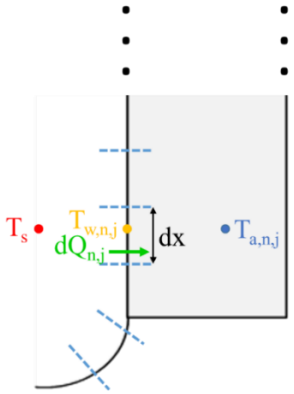

Figure 5: Diagram of model divisions along a condenser cross section, n; not to scale

The thermal model is run independently in each cross section. The scheme of the model is shown in Figure 4. Here, $\overline{h_s}$ is the area-averaged HTC for the entire condenser, h_s is the average HTC for each 1 m measurement section, and $h_{s,n,j}$ is the local HTC over a 1 mm height x 1 m length of condenser. The cross section is discretized into *J* steps of height $dX = 1\text{mm}$, as seen in Figure 5.

Beginning at the tube bottom, where air temperature, T_{ai}, is known, the air HTC is calculated. The profile for air-side HTC along the fin length is calculated from a CFD simulation in the current fin geometry. The result is proportional to the Reynolds number along the fin length:

$$\text{Nu}_{a,\text{n,j}} \propto \text{Re}_{\text{a,n,j}}^{0.7}\,\text{Pr}_{a,\text{n,j}}^{1/3} \tag{30}$$

This profile is then calibrated to match the mean air-side HTC, h_a , for each cross section, as determined from an experimental correlation developed by Wilson plot for this particular condenser by Creative Thermal Solutions, Inc.:

$$\overline{\text{Nu}_a} = 0.2329\,\text{Re}_a^{0.5} \tag{31}:$$

$h_{s,n,j}$ is calculated by one-dimensional conduction through the condensate river, as in equation (32):

$$h_{\text{s,river,n,j}} = \frac{\left(dX - ds_j\right)k_f}{t_{c,\text{n,j}}\,dX\,\ln\left(dX\,/\,ds_j\right)} \tag{32}$$

Local capacity is then found by equation (33):

$$dQ_{n,j} = dUA_{n,j}\left(T_s - T_{a,n,j}\right) \tag{33}$$

$$\frac{1}{dUA_{n,j}} = \frac{1}{h_{a,n,j}\eta_{o,n,j}A_{a,n}} + \frac{t_w}{k_w A_{s,n}} + \frac{1}{h_{s,n,j}A_{s,n}} \tag{34}$$

The three terms on the right-hand side of equation (34) represent the air, wall, and steam heat transfer resistances, respectively. The wall resistance is constant. From the local capacity, the wall temperature and subsequent air temperature can be calculated by equations (35) and (36):

$$T_{w,n,j} = T_{a,n,j} + dQ_{n,j}\left(\frac{1}{h_{a,n,j}A_{a,n}\eta_{o,n,j}}\right) \tag{35}$$

$$T_{a,n,j+1} = T_{a,n,j} + \frac{dQ_{n,j}}{C_{p,a,n,j}\dot{m}_{a,n}} \tag{36}$$

When the model reaches the region above the condensate river, steam-side HTC is determined from Nusselt analysis (Nusselt, 1916). Wall temperature is necessary for calculating this HTC, so the wall temperature from the previous 1 mm section is used:

$$h_{s,n,j} = \left[\frac{i_{fg}g\left(\rho_f - \rho_g\right)k_f{}^3}{4X_j\left(T_s - T_{w,n,j-1}\right)\nu_f}\right]^{1/4} \tag{37}$$

To summarize, the model is calculated by stepping in 1 mm increments from tube bottom to top along the condenser wall (in the X-direction). Steam and air HTC, air and wall temperatures, and capacity are calculated at each increment. At the tube bottom, $h_{s,n,j}$ is determined from a 1-D conduction model through the condensate river (equation (32)). The shape of the condensate river is modeled using the model described in section 3. Above the condensate river, $h_{s,n,j}$ is modeled in the natural-convection film-condensation regime using equation (37).

5. RIVER MODEL RESULTS

5.1 Comparison with Experiment Results

Figure 6 shows the predicted river depth vs the measured depth along the condenser length for three different inclination angles. The model closely matches experiment results. The efficacy of the model can be noted in the ability to predict the unusual profile of the river when the condenser is inclined at $\varphi = 0.3°$. Conventional void fraction correlations cannot predict this void fraction behavior (increase in void fraction near the condenser outlet) that is dependent on the tube outlet condition.

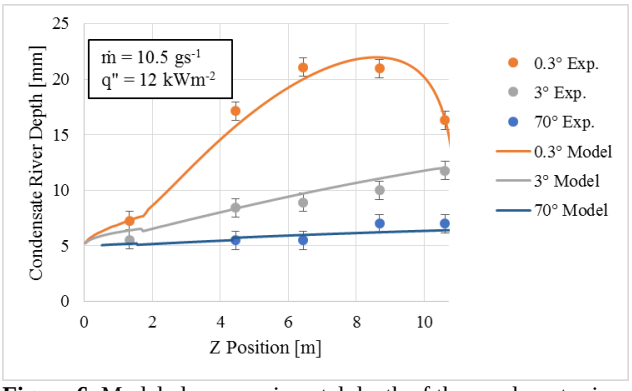

Figure 6: Modeled vs experimental depth of the condensate river along the length of the condenser for three different inclination angles

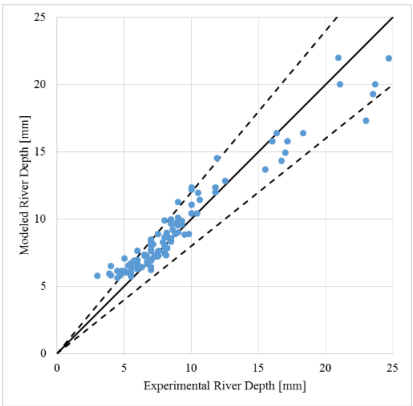

Figure 7: Comparison of modeled condensate river depth to experimental river depth

Figure *7* compares modeled condensate river depth against the experimental data. The model predicts 79% of the data within 20%. The model tends to under-predict the experimental results at high river depths, and over-predict at low river depths.

6. THERMO-HYDRAULIC MODEL RESULTS

6.1 Capacity

The thermal model is validated by comparing the total condenser capacity from the model and from the experiment. Figure 8 shows that all experimental capacities were predicted to within 5% by the model. Similar verifications were performed with capacity of each measurement section, and with condenser *U*, although they are not shown here.

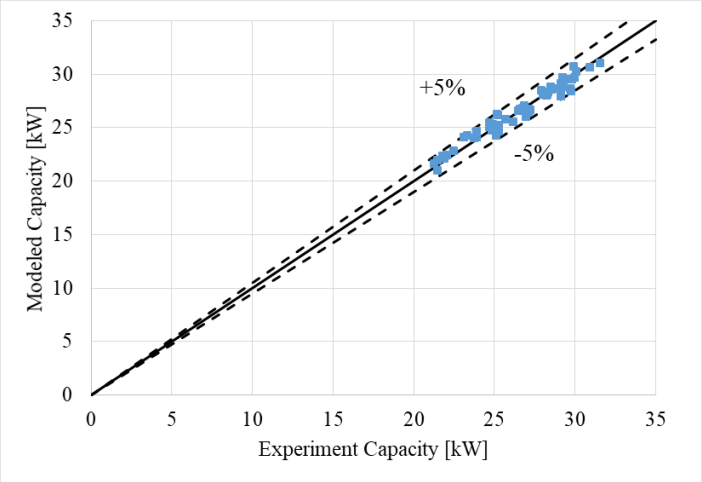

Figure 8: Modeled capacity compared to experiment capacity

6.2 Temperature and Overall Heat Transfer Coefficient

An example of the modeled temperatures is presented in Figure 9. The non-linear temperature profile can be observed. Experiment wall, air, and steam temperatures are also plotted for comparison. The model under-predicts the wall temperature, which indicates that the steam HTC is higher than assumed in the model. This is expected, as the natural-convection model used is a lower bound for HTC in pipe flow. An example of $h_{a,n,j}$ and $h_{s,n,j}$ in a cross section are given in Figure 10. Air-side HTC decreases in the airflow direction as the boundary layer grows. Steam-side HTC decreases from tube top to bottom due to an increase in thickness of the condensate film. The most significant decrease is seen at the bottom, due to the high heat transfer resistance of the condensate river.

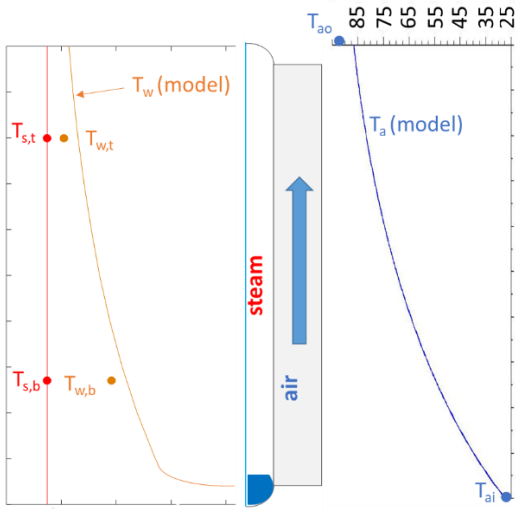

Figure 9: Modeled temperatures, T_w and T_a compared to measured values. Model values are presented by lines while dots are used for measured values

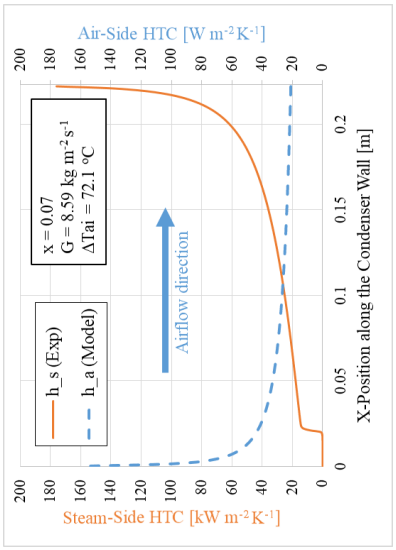

Figure 10: Calibrated model of air- and steam-side HTC along a vertical profile of the condenser tube; Z = 10.5m

7. CONCLUSIONS

A thermo-hydraulic model has been developed to predict capacity, void fraction, and overall heat transfer coefficient of a flattened-tube air-cooled condenser. The hydraulic model accurately predicts the depth of the stratified condensate layer using open-channel-flow theory. The model is particularly accurate at predicting the decrease in condensate depth near the tube outlet of the horizontal condenser. For heat transfer, the model predicts all experiment capacities to within 5%.

NOMENCLATURE

A	Area	m^2	q''	Heat flux	$W\ m^{-2}$
b^2	Capillary constant	m^2	$r(x)$	Local radius of curvature of condensate river surface	m
c_p	Specific heat at constant pressure	$J\ kg^{-1}\ K^{-1}$	R	Resistance to heat transfer	$K\ m^2\ W^{-1}$
C_d	Bulk drag coefficient		R_h	Hydraulic radius	m
D_h	Hydraulic diameter	m	Re	Reynolds number	
f	Friction factor		Re_a	Reynolds number of air, based on hydraulic diameter of channel between fins	
Fr	Froude number		$\mathrm{Re}_{a,j}$	Reynolds number of air, based on distance X along the tube perimeter	
g	Gravitational acceleration	$m\ s^{-2}$	s	Length along condensate surface	m
G	Mass flux	$kg\ m^{-2}\ s^{-1}$	t	Thickness	m
h	Heat transfer coefficient	$W\ m^{-2}\ K^{-1}$	$t_{c,PC}$	Height of the condensate river along the polycarbonate window	m
i	Specific enthalpy	$J\ kg^{-1}$	T	Temperature	^oC
i_{fg}	Specific enthalpy of vaporization	$J\ kg^{-1}$	u	Uncertainty	
k	Thermal conductivity	$W\ m^{-1}\ K^{-1}$	U	Overall heat transfer coefficient, based on air-side area	$W\ m^{-2}\ K^{-1}$
L	Length	m	v	Velocity	$m\ s^{-1}$
$LMTD$	Log mean temperature difference	^oC	$\dot{V}$	Volumetric flow rate	$m^3\ s^{-1}$
$\dot{m}$	Mass flow rate	$kg\ s^{-1}$	X	Position along wall height	m
n	Manning's n		x	Vapor quality	
Nu	Nusselt number		Y	Position perpendicular to wall	m
Pr	Prandtl number		Z	Axial position: z = 0 at tube inlet	m
Q	Heat transferred	W			

Subscripts

a	Air
c	Condensate
cs	Cross section
f	Fluid
$face$	Denotes cross-section between fins
g	Gas
i	Inlet
j	Denotes measurement section in X-direction
n	Denotes measurement section in Z-direction
o	Outlet
PC	Polycarbonate
s	Steam
st	Steel
w	Wall

Greek Symbols

α	Void fraction	
β	Angle between river surface and Y-axis	^{o}
ε	Surface roughness	mm
η	Overall surface efficiency	
μ	Viscosity	$kg\ m^{-1}\ s^{-1}$
ν	Kinematic viscosity	$m^2\ s^{-1}$
ρ	Density	$kg\ m^{-3}$
σ	Surface tension	$N\ m^{-1}$
φ	Inclination angle	^{o}

ACKNOWLEDGEMENTS

The authors thankfully acknowledge the support provided by CTS - Creative Thermal Solutions, Inc., the Air Conditioning and Refrigeration Center, the University of Illinois at Urbana-Champaign, and TechnipFMC.

REFERENCES

Chato, J. C. (1960). *Laminar condensation inside horizontal and inclined tubes.* Massachusetts Institute of Technology.

Chow, V. T. (1959). Open channel hydraulics.

Davies, W. A., Kang, Y., Hrnjak, P., & Jacobi, A. M. (2018). Method for evaluating the effect of inclination on the performance of large flattened-tube steam condensers with visualization of flow regimes. *Applied Thermal Engineering*.

Dobson, M., & Chato, J. (1998). Condensation in smooth horizontal tubes. *Journal of Heat Transfer, 120*(1), 193-213.

Hussein, H., Mohamad, M., & El-Asfouri, A. (2001). Theoretical analysis of laminar-film condensation heat transfer inside inclined wickless heat pipes flat-plate solar collector. *Renewable Energy, 23*(3-4), 525-535.

Kang, Y., Davies III, W. A., Hrnjak, P., & Jacobi, A. M. (2017). Effect of inclination on pressure drop and flow regimes in large flattened-tube steam condensers. *Applied Thermal Engineering*.

Kao, T. (1974). Spatially varied subcritical and supercritical flow in gullies.

Kekaula, K., Chen, Y., Ma, T., & Wang, Q. W. (2017). Numerical investigation of condensation in inclined tube air-cooled condensers. *Applied Thermal Engineering, 118*, 418-429. doi:10.1016/j.applthermaleng.2017.03.001

Li, J., & Hrnjak, P. (2017). Separation in condensers as a way to improve efficiency. *International journal of refrigeration, 79*, 1-9.

Lips, S., & Meyer, J. P. (2012). Stratified flow model for convective condensation in an inclined tube. *International Journal of Heat and fluid flow, 36*, 83-91.

Mills, A. (1962). Experimental investigation of turbulent heat transfer in the entrance region of a circular conduit. *Journal of Mechanical Engineering Science, 4*(1), 63-77.

Nusselt, W. (1916). Die Oberflachenkondesation des Wasserdamffes the surface condensation of water. *Zetrschr. Ver. Deutch. Ing., 60*, 541-546.

Saffari, H., & Naziri, V. (2010). Theoretical modeling and numerical solution of stratified condensation in inclined tubes. *Journal of mechanical science and technology, 24*(12), 2587-2596.

Sparrow, E., Gorman, J., & Abraham, J. (2013). Quantitative assessment of the overall heat transfer coefficient U. *Journal of Heat Transfer, 135*(6), 061102.

Taitel, Y., & Dukler, A. (1976). A model for predicting flow regime transitions in horizontal and near horizontal gas-liquid flow. *AIChE Journal, 22*(1), 47-55.

Taitel, Y., & Dukler, A. (1976). A theoretical approach to the Lockhart-Martinelli correlation for stratified flow. *International Journal of Multiphase Flow, 2*(5-6), 591-595.

Wang, J., & Ma, Y. (1991). Condensation heat transfer inside vertical and inclined thermosyphons. *Journal of Heat Transfer (Transactions of the ASME (American Society of Mechanical Engineers), Series C);(United States), 113*(3).

Yamashita, H., Izumi, R., & Yamaguchi, S. (1977). Performance of the Cross-Flow Heat Exchanger With Variable Physical Properties: 1st Report, in Case Where the Overall Heat Transfer Coefficient Is Variable. *Bulletin of JSME, 20*(146), 1008-1015.

Yen, B. C. (1971). Spatially varied open-channel flow equations.